Experimental and theoretical evidence for an ionic crystal of ammonia at high pressure

S. Ninet,[1,*] F. Datchi,[1] P. Dumas,[2] M. Mezouar,[3] G. Garbarino,[3] A. Mafety,[1] C. J. Pickard,[4] R. J. Needs,[5] and A. M. Saitta[1]

[1]*Institut de Minéralogie, de Physique des Matériaux et de Cosmochimie, Université Pierre et Marie Curie-Paris 6, CNRS UMR 7590, Sorbonne Universités, IRD UMR 206, MNHN, 4 place Jussieu, F-75005, Paris, France*

[2]*Synchrotron SOLEIL, Boîte Postale 48, 91192 Gif Sur Yvette, France*

[3]*European Synchrotron Radiation Facility, Boîte Postale 2220, F-38043 Grenoble Cedex, France*

[4]*Department of Physics and Astronomy, University College London, Gower Street, London WC1E 6BT, United Kingdom*

[5]*Theory of Condensed Matter Group, Cavendish Laboratory, J J Thomson Avenue, Cambridge CB3 0HE, United Kingdom*

(Received 5 July 2013; revised manuscript received 3 April 2014; published 8 May 2014)

We report experimental and theoretical evidence that solid molecular ammonia becomes unstable at room temperature and high pressures and transforms into an ionic crystalline form. This material has been characterized in both hydrogenated (NH_3) and deuterated (ND_3) ammonia samples up to about 180 and 200 GPa, respectively, by infrared absorption, Raman spectroscopy, and x-ray diffraction. The presence of a new strong infrared absorption band centered at 2500 cm^{-1} in NH_3 (1900 cm^{-1} in ND_3) is in line with previous theoretical predictions regarding the ionization of ammonia molecules into NH_2^- and NH_4^+ ions. The experimental data suggest the coexistence of two crystalline ionic forms, which our *ab initio* structure searches predict to be the most stable at the relevant pressures. The ionic crystalline form of ammonia appears stable at low temperatures, which contrasts with the behavior of water in which no equivalent crystalline ionic phase has been found.

DOI: 10.1103/PhysRevB.89.174103 PACS number(s): 62.50.−p, 64.70.kp, 66.30.jp

I. INTRODUCTION

The properties of ammonia at high pressures and temperatures are important in planetary science and chemistry under extreme conditions. Ammonia has a significant cosmic abundance, and it is believed to be a major constituent of the mantles of gas giant planets, such as Neptune and Uranus, and numerous extra solar (exo)planets. The high P-T phase diagrams of ammonia, shown in Fig. 1, and of water have been the subject of recent investigations [1–6], leading to the experimental discovery of a "superionic" phase [2,5] as previously suggested by *ab initio* calculations [7]. The latter is characterized by rapid diffusion of protons through the crystalline nitrogen or oxygen lattice and could be relevant for understanding the magnetic fields of giant icy (exo)planets.

The current study concerns the properties of ammonia at high pressures but at lower temperatures than required for stabilizing the superionic phase. It has long been thought that solid ammonia would evolve similarly to the isoelectronic water ice with pressure. However, the hydrogen bonds in crystalline ammonia are weaker and more distorted than in water ice, and whereas the latter evolves continuously towards a symmetric H-bonded solid at around 100 GPa where protons sit midway between two oxygen atoms, no sign of H-bond symmetrization in ammonia has been found in *ab initio* calculations up to 300 GPa [7–9] or in experiments up to 120 GPa [10–12]. Nonetheless, a recent theoretical study has suggested that the molecular ammonia solid is thermodynamically unstable above about 100 GPa at low temperatures [9] and that it transforms into a crystalline ionic solid phase with a structure of $Pma2$ symmetry consisting of alternate layers of NH_4^+ and NH_2^- ions. This ionic solid has not been observed in experiments so far.

Here, we present a joint experimental and theoretical investigation that provides strong evidence for the existence of an ionic phase of solid ammonia at high pressures. NH_3 and ND_3 samples have been probed at ambient temperatures up to 194 and 184 GPa, respectively, using Raman scattering, infrared (IR) absorption spectroscopy, and x-ray-diffraction techniques. In parallel, *ab initio* theoretical calculations, including new random structure searches, have been carried out in the same pressure range.

II. EXPERIMENTAL AND THEORETICAL METHODS

Liquid NH_3 (99.99%, Air liquide) and ND_3 (99.96%, Eurisotop) samples were loaded in membrane diamond anvil cells at 5 bar and 278 K. We used synthetic type II as diamond anvils (Almax Industries) with flat culets of diameter 75 or 50 μm. The gaskets were made of rhenium. The pressure was determined up to 70 GPa from the wavelength shift of ruby fluorescence using the ruby scale from Dewaele *et al.* [13] and, at higher pressures, from the frequency shift of the first-order Raman band of the diamond anvil tip [14].

IR absorption experiments were performed on the SMIS beamline of the SOLEIL synchrotron facility (Saint-Aubin, France) using the Fourier-transform-IR spectrometer coupled to a vertical microscope. The IR beam was condensed by 15× Cassegrain objectives to a spot of about 25 μm in the focal plane. The sample absorbance is defined as $A = -\log(I/I_0)$, where I is the measured transmitted intensity and I_0 is the intensity of incident light. To correct for the absorption of the diamond anvils and gasket, we used, as I_0, the transmission spectra measured in a separate experiment with similar diamond anvils and gasket dimensions but using N_2 as a sample, which is transparent in the frequency range of interest. Figure 2 shows an example of IR spectra collected from NH_3 and N_2 at the respective pressures of 40 and 43 GPa and the calculated absorbance of the NH_3 sample.

Raman spectra were collected at each pressure step using a DXR Raman spectrometer from Thermo Fisher Scientific with 532-nm exciting laser radiation. Additional Raman

*sandra.ninet@impmc.upmc.fr

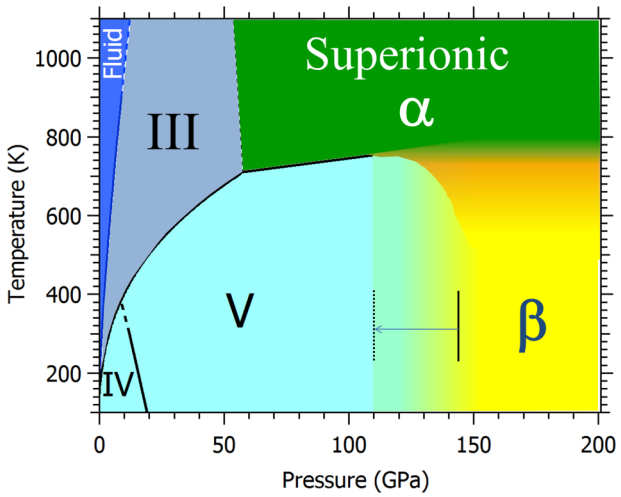

FIG. 1. (Color online) Phase diagram of ammonia. The blue-, blue-gray-, and cyan-colored regions correspond to different molecular phases composed of NH_3 units. The yellow region represents the tentative stability domain of the β phase reported in the present paper, most likely composed of NH_4^+ and NH_2^- species. The solid and dashed lines indicate the upstroke and downstroke transition pressures. At high pressures and temperatures, a dynamic ionization is observed in the superionic α phase [2], which is mainly composed of NH_3, NH_4^+, and NH_2^- species.

spectra were collected with an in-house spectrometer using the 514.5-nm line of an argon laser.

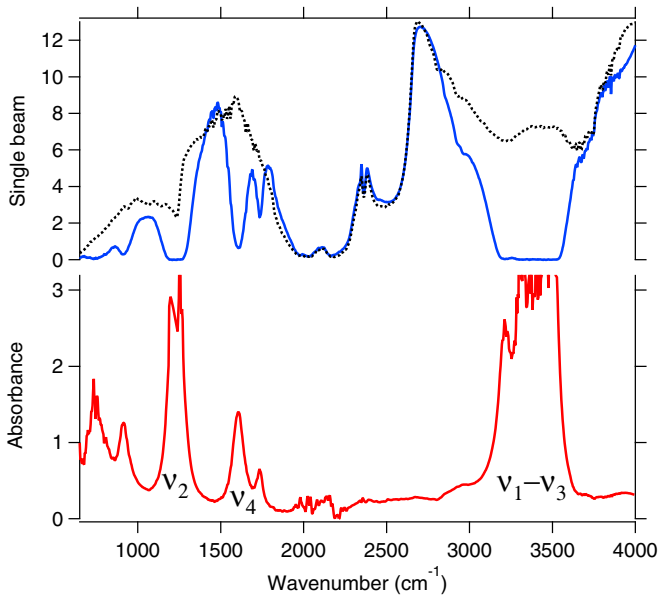

FIG. 2. (Color online) Example of an IR spectrum collected from the molecular phase V ($P2_12_12_1$) of the NH_3 sample at 40 GPa. The upper graph shows the transmission (single beam) spectrum collected from NH_3 at 40 GPa (blue solid curve) and from a N_2 sample at 43 GPa (black dotted curve). The latter is used as the reference spectrum to calculate the absorbance of the NH_3 sample, which is displayed in the lower graph (red solid curve). The internal modes of phase V (ν_1–ν_4) are indicated. The strong absorbance of ν_2 and ν_3 saturates the absorption. The modes below 1000 cm^{-1} are lattice modes.

X-ray-diffraction experiments were conducted at beamline ID27 of the European Synchrotron Radiation Facility [(ESRF) Grenoble, France]. We used the angular-dispersive technique with monochromatic x rays ($\lambda = 0.3738$ Å) and a bidimensional CCD detector (marCCD). The x-ray beam was focused to a spot of size (2×2.6)-μm^2 FWHM on the sample. Integration of the x-ray images was performed with the FIT2D software [15]. Profile refinements were conducted with the FULLPROF software [16].

Crystal structure prediction was carried out using the *ab initio* random structure searching (AIRSS) method [17] and the CASTEP code [18] with up to 12 ammonia formula units and a target pressure of 125 or 150 GPa. Except for the larger number of molecules per unit cell, the same procedure as in Ref. [9] was used. For each phase considered, we calculated the enthalpy/pressure/volume equations of state up to 400 GPa using the PWSF code from the QUANTUM-EXPRESSO distribution [19]. These calculations were performed within a standard density-functional-theory framework using the Perdew-Burke-Ernzerhof (PBE) gradient-corrected functional [20], ultrasoft pseudopotentials [21], and a plane-wave basis set. A kinetic-energy cutoff of 50 Ry and k-point grids typically containing 16–32 points were used. Other functionals also were tested to check the effect on the molecular-ionic transition pressure as explained in the next section. The vibrational modes and corresponding Raman and IR spectra were calculated using the PHONON code from the QUANTUM-EXPRESSO package.

III. RESULTS AND DISCUSSION

Experimental IR and Raman spectra collected on compression of the NH_3 samples are shown in Figs. 3 and 4, respectively. Similar graphs for ND_3 are reported in Figs. 1 and 2 of the Supplemental Material [22]. The vibrational spectrum of the molecular NH_3-V phase is complex with 45 Raman and 35 IR nondegenerate active modes [23]. The strongly absorbing IR bands corresponding to the symmetric bending ($\nu_2 \sim 1450$ cm^{-1} at 137 GPa) and stretching (ν_1–$\nu_3 \sim$ 3000–3500 cm^{-1}) vibrational modes saturate the absorption, even though the sample thickness is very thin at megabar pressures (5–8 μm). By contrast, the antisymmetric bending IR bands (ν_4), Raman-active lattice, and molecular modes of NH_3-V are clearly observed up to 150 GPa. The pressure dependencies of the measured Raman and IR mode frequencies are presented in Figs. 3–5 of the Supplemental Material [22].

Above 150 GPa, strong changes in the experimental IR and Raman spectra are observed, indicating a transition to another high-pressure phase that we refer to as β-NH_3. The latter is characterized by a new strong and broad IR absorption band around 2300–2800 cm^{-1}. The bands in the frequency range corresponding to the bending modes ν_2–ν_4 (from ~1200 to ~1800 cm^{-1}) are also very different from those of phase V. The Raman spectrum exhibits a new peak in the antisymmetric stretching frequency range (around 3700 cm^{-1}), a large decrease in intensity of the strongest peak of phase V (around 3300 cm^{-1}), and the appearance of a broadband around 3000 cm^{-1}. Several new lattice Raman peaks also appear at low frequencies, indicating that the new phase has a larger unit cell than phase V [Fig. 4(c)]. Similar changes are observed in ND_3 above 150 GPa: The new IR bands in ND_3 appear around

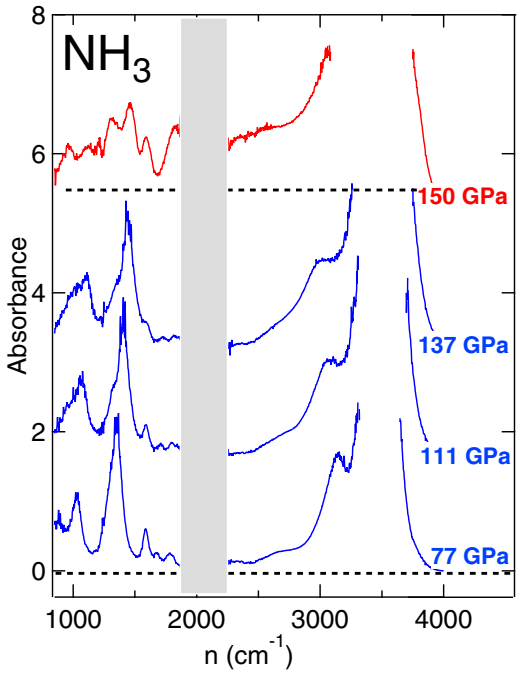

FIG. 3. (Color online) Evolution of the infrared absorption spectra of solid NH_3 with pressure. The spectra have been offset for easier visualization. The blue curves are for the molecular phase V, and the red one is for the β phase. The frequency window from ~2000 to ~2300 cm^{-1} is obscured by the strong absorption band of the diamond anvils. Pressures are indicated on the right.

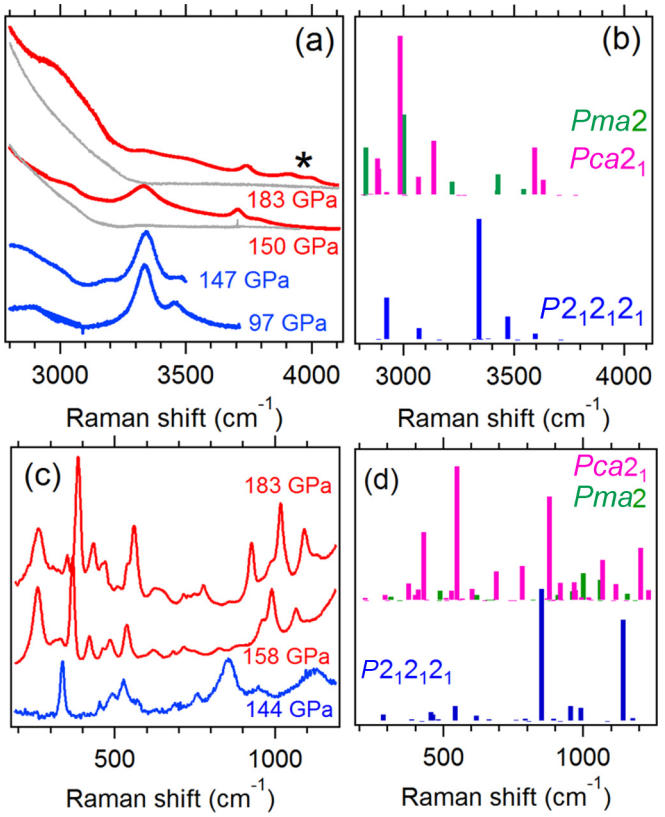

FIG. 4. (Color online) Experimental [(a) and (c) 300 K] and theoretical [(b) and (d) 0 K] Raman spectra of NH_3 are shown across the phase transition between the molecular phase V ($P2_12_12_1$) and the β phase. In (a) and (c), the blue and red curves, respectively, show the experimental spectra below and above the transition at the indicated pressures. The gray curves are spectra recorded with the laser spot focused onto the Re gasket, showing the contribution of the second-order Raman band of the diamond anvils. In (b) and (d), the blue, pink, and green bars, respectively, show the density-functional-perturbation-theory- (DFPT-) predicted Raman modes of the $P2_12_12_1$ phase V at 150 GPa and ionic $Pca2_1$ and $Pma2$ structures at 200 GPa. Global offsets of -100 and -60 cm^{-1} have been applied to the theoretical spectra in (b) and (d), respectively. The star in (a) indicates the two peaks which appeared after exposure to hard x rays (33 keV) and identified as arising from the presence of H_2 (see the text).

1500 cm^{-1} (nonsaturated) and 1800–2000 cm^{-1} (saturated), a new stretching Raman peak appears at ~2750 cm^{-1}, and a broad Raman band is observed around 2000 cm^{-1}.

Note that two other high-frequency Raman peaks, indicated by the star in Fig. 4, appeared after exposure of the NH_3 sample to hard x rays (33 keV) at 183 GPa. These were identified as the stretching vibrations of H_2 in a matrix of ammonia. We interpret this as a partial x-ray-induced decomposition as observed previously in H_2O at lower pressures [24]. No peaks arising from molecular N_2 could be detected, which is not surprising since solid N_2 forms a nonmolecular amorphous state with no Raman-active modes at this pressure [25].

IR and Raman data also were collected on decompression, and the β phase was then observed down to 110 GPa before phase V was recovered. The large hysteresis (40 GPa) between the transitions on the upstroke and downstroke suggests a substantial kinetic barrier between the two phases and, therefore, a likely change in the molecular bonding at the transition.

The theoretical Raman and IR spectra predicted by DFPT for the molecular $P2_12_12_1$ and the $Pma2$ ionic structures [9] are displayed in Figs. 4 and 5, respectively, where they can be compared with the experimental ones. As previously noted, for pressures below 10 GPa [23], DFPT reproduces the experimental Raman mode frequencies of phase V to better than 12%. The comparison is more difficult for the experimental IR spectra because of the overlap of bands and saturation in the spectra. The relative intensities of the theoretical spectra are only in qualitative agreement with experiment. We note that anharmonic effects are not taken into account in the theoretical calculations, which may explain the discrepancies with the experimental data.

The most noticeable difference between the calculated vibrational properties of the $Pma2$ ionic structure and the $P2_12_12_1$ molecular phase is the occurrence in the former of intense IR modes in the region 2460–2700 cm^{-1} at 150 GPa, originating from the vibrations of the NH_4^+ ions [9]. This theoretical prediction gives a good match to our observation of strong IR absorption around 2500 cm^{-1} in the β phase. As an additional check, we calculated the IR and Raman spectra for a number of metastable molecular phases obtained from the structural searches: None of them have vibrational modes in this spectral region. The predicted IR bands of $Pma2$ around 1500–1650 cm^{-1} also agree well with the experiment; however, there is no strong IR absorption predicted for $Pma2$ around 1900 cm^{-1}, in contrast to observations for the β phase,

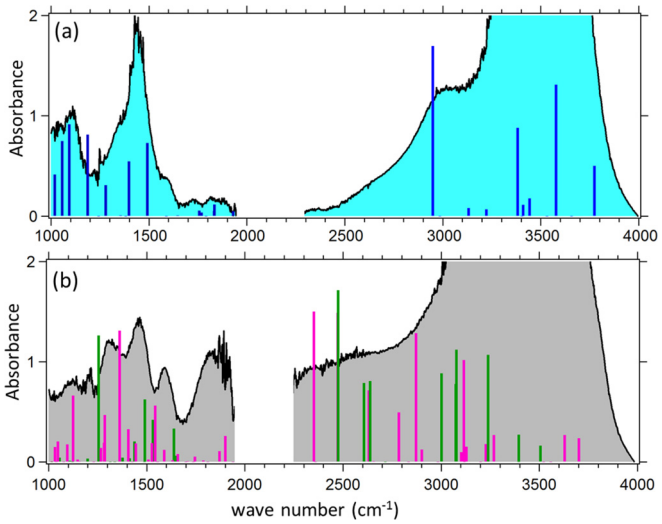

FIG. 5. (Color online) The experimental mid-IR absorption spectra of ammonia are shown at (a) 144 GPa and (b) 158 GPa, respectively, below and above the phase transition at 300 K (black solid curves). The blue, green, and pink bars show the theoretically predicted IR modes at 150 GPa and 0 K of the molecular $P2_12_12_1$, ionic $Pma2$, and $Pca2_1$ structures, respectively. In order to make the lower-frequency bands more visible, the theoretical IR intensities have been multiplied by 6 for mode frequencies below 2000 cm^{-1}.

and the predicted absorption in the range 3000–3700 cm^{-1} is smaller than observed.

In the Raman spectra, the observed decrease in the intensity of the main antisymmetric stretching mode (3400 cm^{-1}) and the increase in intensity around 3000 cm^{-1} are consistent with the predicted Raman features of the $Pma2$ phase. Nevertheless, the newly observed stretching band at about 3700 cm^{-1}, as well as the new lattice modes below 300 cm^{-1}, are absent in the $Pma2$ structure, which suggests that this phase alone cannot account fully for the experimental results.

As seen in Fig. 6(a), there are also some inconsistencies between the measured x-ray diffraction pattern of the β phase at 194 GPa and the calculated one for the $Pma2$ structure. As a matter of fact, although the reflections of the $Pma2$ structure are present in the experimental pattern, there are several other peaks which it cannot account for. These observations suggest a larger unit cell, a lower symmetry, or the coexistence of different structures.

New *ab initio* random structural searches [17] were, therefore, undertaken to determine whether other NH_3 structures could exist in the pressure range of our experimental observations. The same method as in Ref. [9] was used, but the maximum number of NH_3 units per unit cell (Z) was tripled with respect to the previous paper, which used up to four molecular units. These searches found the previously reported [9] $Pma2$ ($Z = 4$) ionic structure and a number of new structures, including an ionic structure of space group $Pca2_1$ with eight formula units. An enthalpy-pressure plot for the most competitive structures is shown in Fig. 7. The $Pma2$ ionic structure is confirmed to be the most stable between 100 and 176 GPa, whereas the $Pca2_1$ ionic structure becomes thermodynamically preferred between 176 and 300 GPa. No lower enthalpy structure was found in searches with 12 formula units. We have checked whether the appearance of a stable ionic phase is robust with respect to the choice of density functional, finding that each functional tested predicts a transition from the molecular phase-V structure ($P2_12_12_1$) to the ionic $Pma2$ structure. The transition pressure, however, varies with the functional chosen, ranging from 68 GPa with local-density approximation (LDA) to 116 GPa with PBE0 [26]. Table I lists the transition pressures for all cases tested, resulting from previous [9,27] or present calculations.

Like $Pma2$, $Pca2_1$ is composed of NH_4^+ and NH_2^- ions, but whereas, $Pma2$ consists of alternate layers of NH_4^+ and NH_2^- and has a pseudo-fcc N lattice, $Pca2_1$ is composed of zig-zag chains with a pseudo-hcp N lattice [Fig. 6(b)]. Another ionic structure of space group $P2_12_12$ ($Z = 8$) also

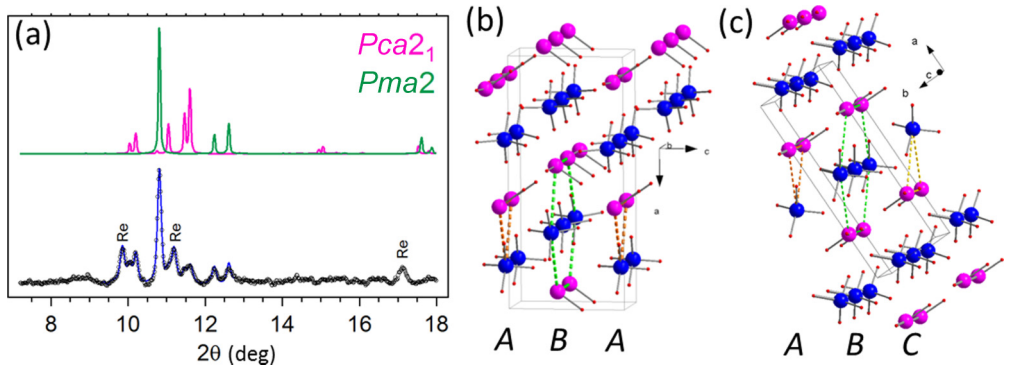

FIG. 6. (Color online) X-ray pattern and structures of ionic ammonia. (a) The experimental (background-subtracted) x-ray pattern from the NH_3 sample at 194 GPa and 300 K is shown as black circles in the lower panel. The blue solid line is a Le Bail refinement obtained by considering a mixture of three phases: $Pma2$, $Pca2_1$, and rhenium from the gasket (peaks indicated by Re). In the upper part, the simulated x-ray powder patterns of the $Pca2_1$ (pink) and $Pma2$ (green) structures are depicted using the cell parameters determined from the Le Bail refinement: $Pma2$: $a = 7.011$ Å, $b = 2.408$ Å, and $c = 2.404$ Å; $Pca2_1$: $a = 8.540$ Å, $b = 2.415$ Å, and $c = 3.883$ Å. (b) and (c) Representations of the ionic $Pca2_1$ and $Pma2$ structures, respectively. Red, blue, and pink balls, respectively, are H atoms and the N atoms of the NH_2^- and NH_4^+ species. The pseudo-hcp ($ABAB\cdots$) or fcc ($ABCABC\cdots$) stacking of the nitrogen lattices are emphasized. The predicted cell parameters at 200 GPa for $Pma2$ are as follows: $a = 6.9756$ Å, $b = 2.371$ Å, and $c = 2.370$ Å; and for $Pca2_1$, they are as follows: $a = 8.471$ Å, $b = 2.380$ Å, and $c = 3.863$ Å. The differences between observed and predicted cell parameters are below 1.5%.

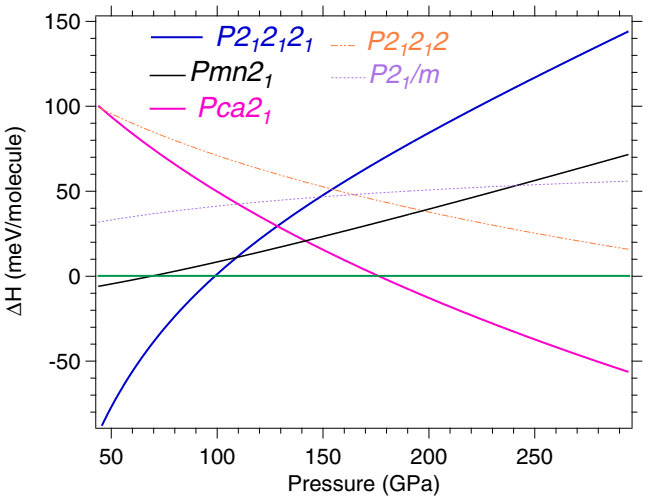

FIG. 7. (Color online) Difference in enthalpy with respect to the ionic $Pma2$ ($Z = 4$) structure as a function of pressure. The $P2_12_12_1$ structure is that of the molecular phase V. The $Pma2$ ionic structure is identical to that reported in Ref. [9]. The other structures were obtained from new structural searches with a larger number of formula units per cell.

was found, which differs from $Pca2_1$ only in the orientation of the NH_2^- ions, but this phase is never stable in the pressure range studied (see Fig. 7). Other very different structures were found: the "mixed" molecular-ionic $Pmn2_1$ structure, composed of NH_4^+, NH_2^- ions and NH_3 molecules and the $P2_1/m$ structure, composed of N^{3-} and NH_4^+ ions. Although unstable at 0 K, these structures are close in enthalpy to the $Pma2$ and $Pca2_1$ phases, especially the mixed $Pmn2_1$ structure, which remains within 25 meV/molecule of the $Pma2$ structure up to ∼160 GPa (see Fig. 7). The structural parameters, representations, and simulated x-ray patterns of all of the phases discussed above are given in Table 1 and Figs. 6 and 7, respectively, of the Supplemental Material [22].

As shown in Fig. 6(a), the experimental x-ray pattern at 194 GPa can be interpreted as arising from the coexistence of the fully ionic $Pma2$ and $Pca2_1$ structures: The fitted unit-cell parameters are within 1.5% of the theoretical ones (see caption for Fig. 6). This coexistence is reasonable as only a small energy separates the two ionic phases over a substantial pressure range around 170 GPa. The x-ray pattern presents too much texture (preferred orientation) to allow the determination of the relative amounts of the two phases from full-profile refinement. Regarding the Raman and IR spectra, the main signature of the ionic species in the $Pca2_1$ structure is, as in $Pma2$, the intense IR modes in the frequency range 2300–2800 cm^{-1} where the molecular phases have no modes at all. In addition, the $Pca2_1$ structure shows strong IR activity around 1900 and 3700 cm^{-1} and two Raman modes around 3600 cm^{-1}, in reasonable agreement with the experimental observations. A coexistence of the two ionic structures, therefore, quantitatively matches the x-ray data and, qualitatively, the Raman and IR data. Clearly, the agreement between the observed and the theoretical intensities for the Raman and IR spectra is poor, but as observed above for the molecular $P2_12_12_1$ phase, this likely originates from the approximations used in the theoretical approach, which is limited to the harmonic level.

TABLE I. Predicted transition pressures between the molecular $P2_12_12_1$ and the ionic $Pma2$ structures according to different DFT functionals: PBE [20], PBE + Tkatchenko-Scheffler van der Waals (TS-vdW) scheme [28], LDA, Heyd-Scuseria-Ernzerhof (HSE) HSE06 [29], and PBE0 [26]. The results of calculations with the PBE, LDA, and PBE0 functionals were reported previously in Refs. [9,27], and those for the PBE + TS-vdW and HSE06 functionals were performed in the present paper. The molecular-ionic transition is predicted in every case.

Functional	PBE	PBE + TS-vdW	LDA	HSE06	PBE0
P (GPa)	97	83	68	126	116

We also considered the possibility of a coexistence of the ionic $Pma2$ and mixed $Pmn2_1$ structures. Since $Pmn2_1$ is partially ionic, its Raman and IR spectra have similar features as the $Pma2$ and $Pca2_1$ structures (see Fig. 8 of the Supplemental Material [22]). The Bragg reflections, which are not indexed by $Pma2$ or the gasket, can also be well indexed by $Pmn2_1$ (see Fig. 9 of the Supplemental Material [22]); however, the ratios of the refined cell parameters for the $Pmn2_1$ structure are $b/a = 1.103$ and $c/a = 1.248$, which are quite different from the theoretical ones: $b/a = 1.046$ and $c/a = 1.221$. Since, according to our calculations, the $Pmn2_1$ structure does not have a pressure range of thermodynamic stability, this coexistence model, thus, appears less likely. The same arguments also militate against coexistence of the molecular $P2_12_12_1$ phase with $Pma2$ at this pressure. Indeed, the theoretical b/a and c/a ratios for $P2_12_12_1$ at 200 GPa are 1.736 and 1.631, respectively. These agree well with the extrapolation of experimental data [11] up to 120 GPa and differ substantially from the cell axis ratios which are obtained from our x-ray pattern at 194 GPa. Moreover, the enthalpy difference between $P2_12_12_1$ and $Pca2_1$ increases rapidly with pressure and exceeds 0.1 eV/molecule at 200 GPa.

Of course, we cannot exclude the possibility that another structure with a larger unit cell, that could result from a more complex stacking sequence of the ionic planes than fcc or hcp, might explain the experimental data. As mentioned above though, no molecular structure found in our searches up to 12 formula units exhibits IR absorption in the spectral range around 2500 cm^{-1}, making a strong case that the β phase is, at least, partially ionic.

It is interesting to note that all of the crystalline phases of ammonia have a nitrogen sublattice that can be described as pure, pseudo-hcp, or fcc. This is the case for the proton-disordered molecular phases II (hcp) and III (fcc) and the proton-ordered molecular phases I (pseudo-fcc), IV, and V (pseudo-hcp). Even the high P-T superionic α phase may have either a fcc or a pseudo-hcp N lattice, depending on whether it is obtained by compressing phase III or annealing phase V, respectively [2]. Our findings extend this property to the low-temperature ionic phases $Pma2$ (pseudo-fcc) and $Pca2_1$ (pseudo-hcp). Since the N atoms already adopt densely packed configurations and are clearly reluctant to undergo a rearrangement, the "job" of minimizing the energy as density increases is accomplished by rearrangements of the H atoms.

As pointed out in Ref. [9], the volumes per formula unit of the ionic phases are much smaller than in the molecular ones because the shapes of the NH_4^+ and NH_2^- ions enable them to pack more tightly than NH_3 molecules. The ionic structures are, therefore, favored at high density. We also note that the $Pca2_1$ structure strongly resembles the $P2_1/m$ ionic phase predicted to be stable above 300 GPa [9] where NH_2^- ions are linked in zig-zag chains by symmetric H bonds.

IV. CONCLUSION

To summarize, our experimental investigation of solid ammonia at pressures of nearly 200 GPa shows that a transition to a previously unobserved phase, denoted β, occurs at 150 GPa on compression, which remains stable down to 110 GPa on decompression. The important changes in the Raman and IR active internal modes with respect to the molecular phase V indicate a drastic modification of the intramolecular bonding across the transition. The appearance of intense IR bands in the frequency range around 2500 cm^{-1} makes a strong case in favor of an ionic structure for the β phase, composed of NH_4^+ and NH_2^- ions as predicted in a previous theoretical paper [9]. The latter has been expanded in the present study with two main additional results: First, the predicted transition between the molecular $P2_12_12_1$ and the ionic $Pma2$ around 100 GPa is proved to be robust against the choice of density functional. Second, our new structural searches with up to 12 formula units per unit cell demonstrate that $Pma2$ remains the most competitive phase above 100 GPa at 0 K and that another ionic structure with space group $Pca2_1$ ($Z = 8$) becomes more stable above 176 GPa. The experimental Raman, IR, and x-ray data are best explained by a coexistence of the $Pma2$ and $Pca2_1$ ionic structures near 190 GPa, which is consistent with the small enthalpy difference ($\sim$15 meV/molecule) between the two phases. Although we cannot presently exclude the possibility that the β phase has a different crystallographic structure with perhaps a larger number of formula units per unit cell, the presence of strong IR absorption in the range of NH_4^+ vibrations suggests that this structure is composed, at least partially, of ionic species.

Our results confirm that, despite their resemblance at ambient and moderate pressures, NH_3 and H_2O follow different structural evolutions at very high densities; whereas ammonia transforms from a molecular to an ionic ammonium amide solid at megabar pressures, water ice evolves into a symmetric H-bonded solid in the same pressure range. In Ref. [9], it was pointed out that the cost of forming a solid composed of H_3O^+ and OH^- units is larger than for solid ammonium amide (1.5 and 0.9 eV/unit, respectively). This adds to the fact that water ice can form compact structures accommodating strong and symmetric H bonds, whereas, in ammonia ice, the close-packed N lattice leads to weaker and inequivalent H bonds that cannot symmetrize without a large deformation of the molecules [30]. We also note that mixtures of ammonia and water have been predicted to form ionic ammonium hydroxide solids under pressure [27]. It would be interesting to extend the present work in this direction, especially since ammonia hydrates are relevant for the descriptions of icy planets and their moons. Finally, further investigations are required to understand the relationship between the static ionic solid found here and the dynamic superionic one reported in Ref. [2] at high P-T conditions.

ACKNOWLEDGMENTS

We acknowledge the synchrotron SOLEIL for provision of beam time allocated on the SMIS beamline to Proposals No. 20090281, No. 20110969 and No. 20120599 and the ESRF for in-house beam time at ID27. The computational part of this work was performed using HPC resources from GENCI/IDRIS (Grant No. 2012-091387). We thank S. Petit Girard (ESRF-ID27) and G. Weck (CEA) for their help with the x-ray experiments and C. Sandt, F. Jamme (SOLEIL-SMIS) and F. Occelli (CEA) for their help with the IR experiments. C.J.P. and R.J.N. acknowledge financial support from the EPSRC.

[1] S. Ninet and F. Datchi, J. Chem. Phys. **128**, 154508 (2008).
[2] S. Ninet, F. Datchi, and A. M. Saitta, Phys. Rev. Lett. **108**, 165702 (2012).
[3] J. G. O. Ojwang, R. S. McWilliams, X. Ke, and A. F. Goncharov, J. Chem. Phys. **137**, 064507 (2012).
[4] M. Bethkenhagen, M. French, and R. Redmer, J. Chem. Phys. **138**, 234504 (2013).
[5] A. F. Goncharov, N. Goldman, L. E. Fried, J. C. Crowhurst, I-F. W. Kuo, C. J. Mundy, and J. M. Zaug, Phys. Rev. Lett. **94**, 125508 (2005).
[6] J. F. Lin, E. Gregoryanz, V. V. Struzhkin, M. Somoayazulu, H. K. Mao, and R. J. Hemley, Geophys. Res. Lett. **32**, L11306 (2005).
[7] C. Cavazzoni, G. L. Chiarotti, S. Scandolo, E. Tosatti, M. Bernasconi, and M. Parrinello, Science **283**, 44 (1999).
[8] A. D. Fortes, J. P. Brodholt, I. G. Wood, and L. Vočadlo, J. Chem. Phys. **118**, 5987 (2003).
[9] C. J. Pickard and R. J. Needs, Nat. Mater. **7**, 775 (2008).
[10] M. Sakashita, H. Yamawaki, H. Fujihisa, and K. Aoki, Rev. High Pressure Sci. Technol. **7**, 796 (1998).
[11] F. Datchi, S. Ninet, M. Gauthier, A. M. Saitta, B. Canny, and F. Decremps, Phys. Rev. B **73**, 174111 (2006).
[12] S. Ninet, F. Datchi, S. Klotz, G. Hamel, J. S. Loveday, and R. J. Nelmes, Phys. Rev. B **79**, 100101(R) (2009).
[13] A. Dewaele, P. Loubeyre, and M. Mezouar, Phys. Rev. B **70**, 094112 (2004).
[14] P. Loubeyre, F. Occelli, and R. LeToullec, Nature (London) **416**, 613 (2002).
[15] A. Hammersley, S. O. Svensson, M. Hanfland, A. Fitch, and D. Hausermann, High Pressure Res. **14**, 235 (1996).
[16] J. Rodriguez-Carvajal, Physica B **192**, 55 (1993), see http://www.ill.eu/sites/fullprof//.
[17] C. J. Pickard and R. J. Needs, J. Phys.: Condens. Matter **23**, 053201 (2011).
[18] S. J. Clark, M. D. Segall, C. J. Pickard, P. J. Hasnip, M. I. J. Probert, K. Refson, and M. C. Payne, Z. Kristallogr. **220**, 567 (2005).

[19] P. Giannozzi *et al.*, J. Phys.: Condens. Matter **21**, 395502 (2009).
[20] J. P. Perdew, K. Burke, and M. Ernzerhof, Phys. Rev. Lett. **77**, 3865 (1996).
[21] D. Vanderbilt, Phys. Rev. B **41**, 7892 (1990).
[22] See Supplemental Material at http://link.aps.org/supplemental/10.1103/PhysRevB.89.174103 for additional figures and table.
[23] S. Ninet, F. Datchi, A. M. Saitta, M. Lazzeri, and B. Canny, Phys. Rev. B **74**, 104101 (2006).
[24] W. L. Mao, H. K. Mao, Y. Meng, P. J. Eng, M. Y. Hu, P. Chow, Y. Q. Cai, J. Shu, and R. J. Hemley, Science **314**, 636 (2006).
[25] E. Gregoryanz, A. F. Goncharov, R. J. Hemley, and H. K. Mao, Phys. Rev. B **64**, 052103 (2001).
[26] C. Adamo and V. Barone, J. Chem. Phys. **110**, 6158 (1999).
[27] G. I. G. Griffiths, R. J. Needs, and C. J. Pickard, Phys. Rev. B **86**, 144102 (2012).
[28] A. Tkatchenko and M. Scheffler, Phys. Rev. Lett. **102**, 073005 (2009).
[29] A. V. Krukau, O. A. Vydrov, A. F. Izmaylov, and G. E. Scuseria, J. Chem. Phys. **125**, 224106 (2006).
[30] M. Gauthier, P. Pruzan, J. C. Chervin, and J. M. Besson, Phys. Rev. B **37**, 2102 (1988).